

LETTERS

A reversible wet/dry adhesive inspired by mussels and geckos

Haeshin Lee¹, Bruce P. Lee⁴ & Phillip B. Messersmith^{1,2,3}

The adhesive strategy of the gecko relies on foot pads composed of specialized keratinous foot-hairs called setae, which are subdivided into terminal spatulae of approximately 200 nm (ref. 1). Contact between the gecko foot and an opposing surface generates adhesive forces that are sufficient to allow the gecko to cling onto vertical and even inverted surfaces. Although strong, the adhesion is temporary, permitting rapid detachment and reattachment of the gecko foot during locomotion. Researchers have attempted to capture these properties of gecko adhesive in synthetic mimics with nanoscale surface features reminiscent of setae^{2–7}; however, maintenance of adhesive performance over many cycles has been elusive^{2,8}, and gecko adhesion is greatly diminished upon full immersion in water^{9,10}. Here we report a hybrid biologically inspired adhesive consisting of an array of nanofabricated polymer pillars coated with a thin layer of a synthetic polymer that mimics the wet adhesive proteins found in mussel holdfasts. Wet adhesion of the nanostructured polymer pillar arrays increased nearly 15-fold when coated with mussel-mimetic polymer. The system maintains its adhesive performance for over a thousand contact cycles in both dry and wet environments. This hybrid adhesive, which combines the salient design elements of both gecko and mussel adhesives, should be useful for reversible attachment to a variety of surfaces in any environment.

The adhesive forces of the gecko have been observed to be on the order of 40 μN or more per seta^{11,12} and 10 nN per spatula¹³. Gecko adhesion has been explained as arising from weak secondary bond forces such as van der Waals¹¹. However, adhesion of a single spatula varies as a function of humidity and is dramatically reduced under water^{9,10}, suggesting some contribution from capillary forces. Contact mechanics arguments have been invoked to explain the subdivision of the setal contact surface into multiple independent nanosized spatulae, giving rise to enhancement of the mechanical behaviour¹⁴. Although the scaling depends on contact geometry, for the idealized case of a hemispherical contact, the theory suggests that the adhesion strength scales with $n^{1/2}$, where n is the number of independent contacts into which the area is subdivided. The contact splitting theory qualitatively explains the scaling of dry adhesive systems used by some amphibians and insects, and provides guidance for development and optimization of synthetic gecko mimics^{2,6,15,16}. Synthetic gecko adhesives that exhibit dry adhesion have been fabricated from polymers^{2–4} as well as multiwalled carbon nanotubes⁵. However, maintenance of adhesion during repetitive contacts has only been demonstrated for a few contact cycles^{2,8}, and none have been shown to function under water.

A celebrated biological model for wet adhesion is the mussel, which is well known for its ability to cling to wet surfaces^{17,18}. Mussels secrete specialized adhesive proteins containing a high content of the catecholic amino acid 3,4-dihydroxy-L-phenylalanine

(DOPA)^{19–21}. Both natural and synthetic adhesives containing DOPA and its derivatives have demonstrated strong interfacial adhesion strength^{22–25}. Using single-molecule measurements in aqueous media, we recently demonstrated that DOPA formed extraordinarily strong yet reversible bonds with surfaces²⁶. In fact, the force necessary to dissociate DOPA from an oxide surface (~ 800 pN) was the highest ever observed for a reversible interaction between a small molecule and a surface²⁶. We speculated that the incorporation of mussel-mimetic polymers into a gecko-foot-mimetic nanoadhesive would yield strong yet reversible wet/dry adhesion—a property that existing materials do not exhibit.

Our strategy employed arrays of gecko-mimetic nanoscale pillars coated with a thin mussel-mimetic polymer film (Fig. 1). The designs of both pillar array and coating polymer incorporated our current knowledge of the respective adhesive systems of gecko and mussel. For the pillar array, the primary design criteria include dimensions of

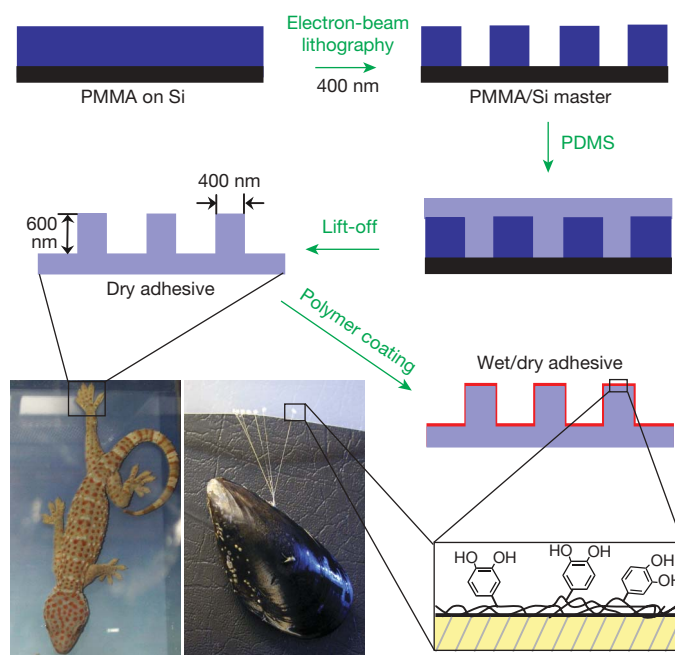


Figure 1 | Rational design and fabrication of wet/dry hybrid nanoadhesive. Electron-beam lithography was used to create an array of holes in a PMMA thin film supported on Si (PMMA/Si master). PDMS casting onto the master is followed by curing, and lift-off resulted in gecko-foot-mimetic nanopillar arrays. Finally, a mussel-adhesive-protein-mimetic polymer is coated onto the fabricated nanopillars. The topmost organic layer contains catechols, a key component of wet adhesive proteins found in mussel holdfasts.

¹Biomedical Engineering Department, ²Material Science and Engineering Department, ³Institute for BioNanotechnology in Medicine, Northwestern University, Evanston, Illinois 60208, USA. ⁴Nerites Corporation, 525 Science Drive, Suite 215, Madison, Wisconsin 53711, USA.

the pillars and their spacing, as well as the stiffness of the material^{2,15,16}. For flexibility in adapting to rough surfaces, both the supporting substrate and the pillar material were fabricated from poly(dimethylsiloxane) (PDMS) elastomer, which is a well-known organic material with a long history of use in microfabrication²⁷. We successfully fabricated (Fig. 1) arrays of PDMS pillars 200, 400 and 600 nm in diameter, with 1–3 μm centre-to-centre distance, and 600–700 nm in height, using electron-beam lithography. The pillar arrays are supported on a continuous film of PDMS (2–3 mm in thickness), with each PDMS pillar representing a single spatula found at the surface of a gecko foot (Fig. 2a, b). Pillar arrays of 400 nm diameter and 600 nm height were tested for adhesion.

Inspection of mussel adhesive protein composition gave insight into a rational design for a mussel-mimetic polymer. First, the synthetic polymer should have a high catechol content since DOPA accounts for as much as 27% of amino acids in the adhesive proteins found at the interface between mussel byssal pads and their substrate²¹. Second, long-lasting waterproof adhesion requires polymers with low water solubility to prevent their loss into the aqueous medium²⁸. Thus, we synthesized poly(dopamine methacrylamide-co-methoxyethyl acrylate) (p(DMA-co-MEA); Fig. 2c) through free-radical polymerization where the adhesive monomer, DMA, accounts for 17% of this copolymer by weight (¹H-nuclear magnetic resonance spectroscopy). p(DMA-co-MEA) has a high molecular mass and is insoluble in water.

p(DMA-co-MEA) was applied to the PDMS pillar array by dip coating in an ethanol solution of p(DMA-co-MEA). X-ray photoelectron spectroscopy analysis of the coated substrate indicated a thin coating (<20 nm) as demonstrated by the presence of both silicon (103 eV, Si 2p) from PDMS and nitrogen (399 eV, N 1s) from p(DMA-co-MEA) (Supplementary Fig. 1). A thin coating was desired for minimizing the change in pillar dimensions during coating, which was confirmed by scanning electron microscopy after coating with p(DMA-co-MEA) (Fig. 2d). We refer to the resulting

flexible organic nanoadhesive as ‘geckel’, reflecting the inspiration from both gecko and mussel.

The performance of geckel adhesive was evaluated using an atomic force microscopy (AFM) system fully integrated with optical microscopy, which permitted simultaneous measurement of the adhesive contact force along with clear visualization of nanoscale contact area down to the single pillar level. In a typical adhesion experiment (Fig. 3), the AFM piezo was used to bring a tipless cantilever (Si_3N_4) into contact with the geckel pillar array, and upon retraction the force necessary to separate the cantilever from the pillar array was measured. Furthermore, independently changing the spacing d between pillars ($d = 1, 2$ and $3 \mu\text{m}$) and the angle of orientation θ between the pillar array and the cantilever axis (Fig. 3b) allowed us to control the number of pillars contacting the cantilever precisely from one to six. For example, a geckel adhesive with $d = 3 \mu\text{m}$ and $\theta = 45^\circ$ resulted in a single pillar contact (Fig. 3c), whereas $d = 1 \mu\text{m}$ and $\theta = 0^\circ$ resulted in six pillars interacting with the cantilever simultaneously (Fig. 3d, Supplementary Video 1).

Adhesion experiments were performed both in air and under water for uncoated (hereafter ‘gecko’) and p(DMA-co-MEA) coated (‘geckel’) pillar arrays (Fig. 4). Pillar-resolved (that is, area-defined) force measurements showed strong adhesive forces when the cantilever is pulled away from the pillar surface. Figures 4a and b show typical force–distance curves, with each curve representing a specific number (1 to 6) of 400 nm diameter pillars interacting with the Si_3N_4 cantilever surface. The pull-off force was determined from each force–distance curve and mean values from multiple experiments plotted in Fig. 4d as a function of the number of contacting pillars. The observed linear increase in force with pillar number indicates constructive force accumulation, that is, simultaneous detachment of individual pillars from the cantilever. The adhesive force per pillar (Fig. 4e) was calculated from the individual slopes: $39.8 \pm 2 \text{ nN}$ (gecko in air), $5.9 \pm 0.2 \text{ nN}$ (gecko in water), $120 \pm 6 \text{ nN}$ (geckel in air) and $86.3 \pm 5 \text{ nN}$ (geckel in water).

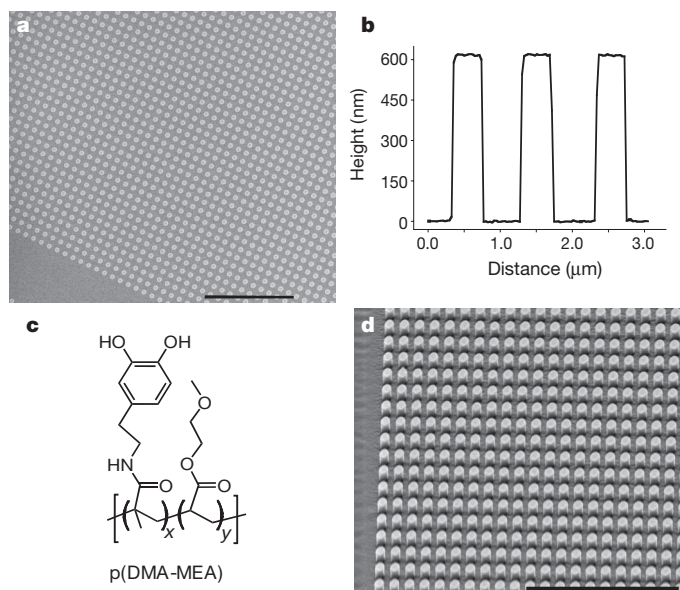


Figure 2 | Fabricated gecko and geckel adhesives. **a**, Scanning electron microscopy image of gecko nanopillar array fabricated using electron-beam lithography. Scale = 10 μm . **b**, AFM linescan of the gecko nanopillars. The height and diameter of the pillars used in this study were 600 and 400 nm, respectively. The apparent widening of the pillars near the base is believed to be an artefact arising from the pyramidal shape of the AFM tip used for imaging. **c**, Chemical structure of the mussel-mimetic polymer, p(DMA-co-MEA), which is applied to the surface of the gecko nanopillars. **d**, Scanning electron microscopy image of geckel adhesive after coating nanopillar array with p(DMA-co-MEA). Scale = 10 μm .

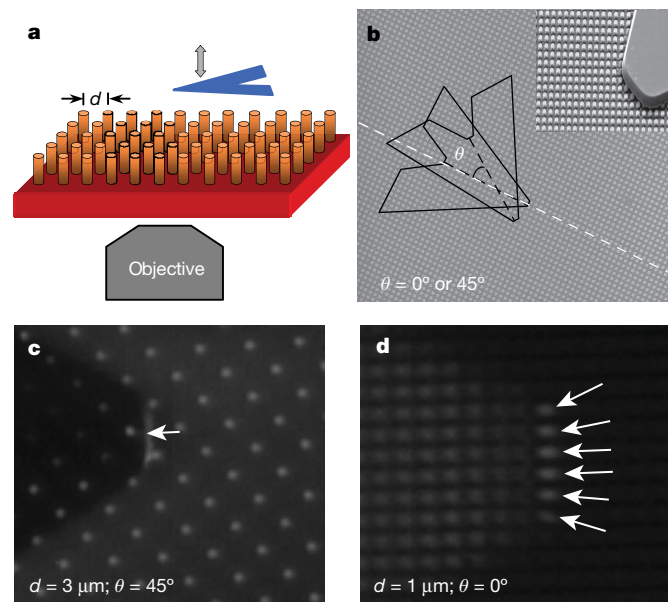


Figure 3 | AFM method for adhesion measurement and imaging of contact area at the single pillar level. **a**, Adhesion was measured by bringing a tipless AFM cantilever into contact with the nanopillar array and then retracting while the contact area is imaged from below. **b**, The number of pillars contacting the cantilever was controlled through the distance d between pillars, and the angle θ between the cantilever and the axis of the pillar array. The inset shows a scanning electron microscopy image of a cantilever contacting a pillar array. **c**, **d**, Optical microscope images showing one (**c**) and six (**d**) pillar contacts achieved with $d = 3 \mu\text{m}$ and $\theta = 45^\circ$, and $d = 1 \mu\text{m}$ and $\theta = 0^\circ$, respectively.

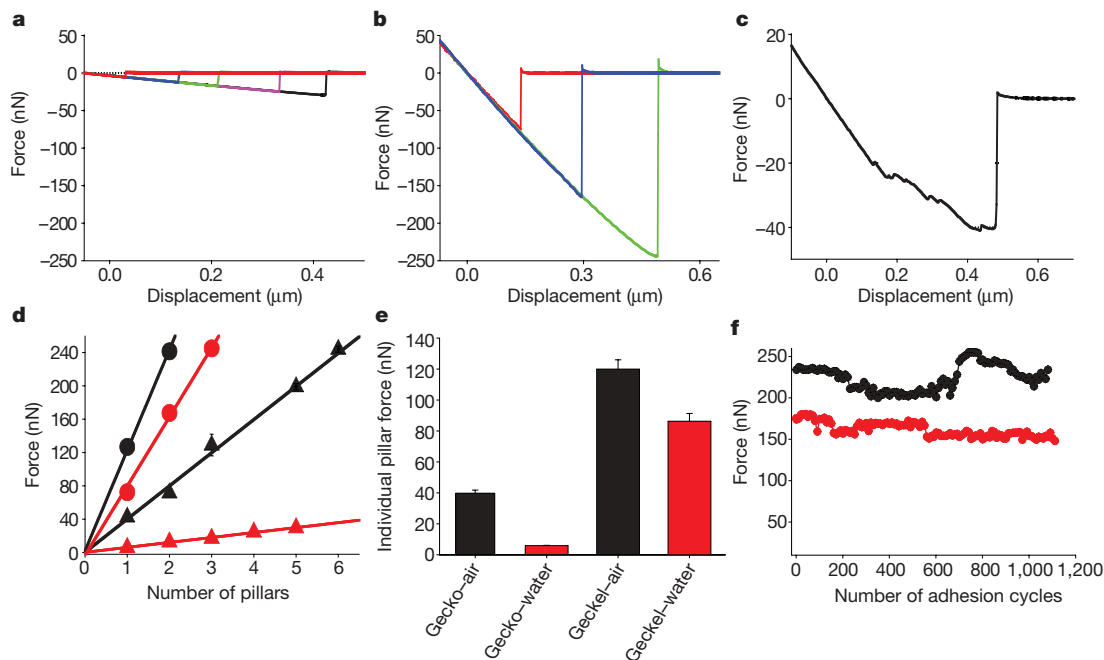


Figure 4 | Force–distance curves and adhesion strength of geckel adhesive. All data are for contact with a Si_3N_4 cantilever. **a, b**, Retraction force–distance curves for uncoated (**a**) and p(DMA-co-MEA) coated (**b**) pillars in water. Force–distance curves were obtained for contact with one (red), two (blue), three (green), four (pink), and five (black) pillars. **c**, Retraction force–distance curve for contact between cantilever and flat

Although the addition of p(DMA-co-MEA) coating on the pillars significantly increased dry adhesion, the enhancement of wet adhesion was particularly dramatic, as the wet adhesive force per pillar increased nearly 15 times (from 5.9 to 86.3 nN per pillar, Si_3N_4) when coated with p(DMA-co-MEA). The geckel wet-adhesion strength was also high when tested against other surfaces: titanium oxide (130.7 ± 14.3 nN per pillar) and gold (74.3 ± 4.1 nN per pillar) (Supplementary Fig. 2). The versatility of geckel is not surprising given recent single-molecule force experiments showing the ability of DOPA to interact strongly with both organic and inorganic surfaces²⁶. These interactions can take many forms, including metal coordination bonds, pi electron interactions, and covalent bonds. The lower adhesion strength of geckel on gold is in qualitative agreement with our earlier single-molecule pull-off and polymer adsorption studies that indicated DOPA interacts less strongly to gold than to titanium oxide^{26,29}.

Furthermore, as suggested by our previous study in which we observed the strong bond between DOPA and a metal oxide surface to rupture upon pulling and then re-form when brought back into contact with the surface²⁶, we speculated that geckel hybrid nanoadhesive may exhibit reversible adhesion to substrates. Repetitive AFM force measurements showed that geckel's wet- and dry-adhesion power was only slightly diminished during many cycles of adhesion, maintaining 85% in wet (red) and 98% in dry (black) conditions after 1,100 contact cycles (Fig. 4f). To our knowledge, no other gecko-mimetic adhesive has demonstrated efficacy for more than a few contact cycles^{2,8}, and none have been shown to work under water. Control experiments involving pillar arrays coated with the catechol-free polymer p(MEA) showed lower adhesion strength (26 nN per pillar for the first contact cycle) as well as rapid decay in the adhesion performance under cyclic testing (Supplementary Fig. 3), emphasizing the importance of the mussel-mimetic catechol groups in enhancing wet adhesion as well as anchoring the p(DMA-co-MEA) polymer on the pillar array. At the same time, it appears that the nanostructured surface is essential to the observed geckel adhesive behaviour. Force measurements on flat substrates coated with

p(DMA-co-MEA)-coated PDMS (contact area = $5.3 \mu\text{m}^2$). **d**, Mean separation force values versus number of pillars for gecko (triangle) and geckel (circle) in water (red) and air (black) ($n > 60$, for each data point). **e**, Adhesion force per pillar, obtained from the slopes of the regression lines shown in **d**. **f**, Performance of geckel adhesive during multiple contact cycles in water (red) and air (black). Error bars represent standard deviation.

p(DMA-co-MEA) indicated a complex peeling behaviour initiating at low adhesive strength (Fig. 4c), which contrasts with the linear force accumulation behaviour exhibited by the geckel adhesive (Fig. 4d).

The geckel nanoadhesive was shown to be highly effective at adhering reversibly to surfaces under water, and with functional performance resembling that of a sticky note. Although we must be cautious in extrapolating our results to larger areas because of the challenges associated with maintaining equal load sharing among a large number of posts, in its current form (400 nm pillar diameter and 1 μm spacing) a 1 cm^2 surface area of geckel adhesive would transmit 9 N of force under water (90 kPa). It is interesting to note that this value is similar to estimates for the strength of gecko dry adhesion^{9,11,12}, suggesting that under wet conditions our hybrid geckel adhesive may perform as well as gecko adhesives do under dry conditions. Further refinement of the pillar geometry and spacing, the pillar material, and mussel-mimetic polymer may lead to even greater improvements in performance of this nanostructured adhesive. The results of this study should be of relevance to the design of wet temporary adhesives for medical, industrial, consumer and military settings.

METHODS SUMMARY

For the fabrication of gecko-mimetic adhesive, we first used electron-beam lithography to create a pattern of holes in a poly(methyl methacrylate) (PMMA) film supported on a silicon wafer (negative mould). To create a gecko-mimetic pillar array, sol phase PDMS was cast onto the negative mould, thermally solidified, and then lifted off from the substrate to yield a positive array of PDMS pillars (~400 nm in diameter and 600 nm in height) supported on a continuous PDMS film. Mussel-mimetic polymer, p(DMA-co-MEA), was synthesized by free radical copolymerization of the DMA and MEA monomers, and its molecular weight was analysed by gel permeation chromatography (Wyatt Technology). Finally, the geckel adhesive was prepared by dip-coating PDMS pillar arrays into an ethanol solution of p(DMA-co-MEA) for 3 h. Surface chemical compositions were analysed by X-ray photoelectron spectroscopy (Omicron) and time-of-flight secondary ion mass spectrometry (ToF-SIMS, Physical Electronics). Pillar arrays were imaged by AFM (Veeco) and scanning electron microscopy (FEI). Adhesive forces under dry/wet conditions were

determined by AFM (MFP-1D, Asylum Research) equipped with tipless cantilevers. The contact area between tip and pillar array was precisely controlled by the distance between pillars ($d = 1, 2$ and $3 \mu\text{m}$) and the angle between cantilever and pillar axis (θ), and was determined by optical imaging using a $40\times$ objective and fibre-optic illumination.

Full Methods and any associated references are available in the online version of the paper at www.nature.com/nature.

Received 2 November 2006; accepted 30 May 2007.

- Ruibal, R. & Ernst, V. The structure of the digital setae of lizards. *J. Morphol.* **117**, 271–293 (1965).
- Geim, A. K. *et al.* Microfabricated adhesive mimicking gecko foot-hair. *Nature Mater.* **2**, 461–463 (2003).
- Northen, M. T. & Turner, K. L. A batch fabricated biomimetic dry adhesive. *Nanotechnology* **16**, 1159–1166 (2005).
- Sitti, M. & Fearing, R. Synthetic gecko foot-hair micro/nano-structures as dry adhesives. *J. Adhes. Sci. Technol.* **17**, 1055–1073 (2003).
- Yurdumakan, B., Ravavikar, N. R., Ajayan, P. M. & Dhinojwala, A. Synthetic gecko foot-hairs from multiwalled carbon nanotubes. *Chem. Commun.* **30**, 3799–3801 (2005).
- Peressadko, A. & Gorb, S. N. When less is more: Experimental evidence for tenacity enhancement by division of contact area. *J. Adhesion* **80**, 1–5 (2004).
- Crosby, A. J., Hageman, M. & Duncan, A. Controlling polymer adhesion with “Pancakes”. *Langmuir* **21**, 11738–11743 (2005).
- Northen, M. T. & Turner, K. L. Meso-scale adhesion testing of integrated micro- and nano-scale structures. *Sensors Actuators A* **130–131**, 583–587 (2006).
- Huber, G. *et al.* Evidence for capillary contributions to gecko adhesion from single spatula nanomechanical measurements. *Proc. Natl Acad. Sci. USA* **102**, 16293–16296 (2005).
- Sun, W., Neuzil, P., Kustandi, T. S., Oh, S. & Samper, V. D. The nature of the gecko lizard adhesive force. *Biophys. J.* **89**, L14–L16 (2005).
- Autumn, K. *et al.* Evidence for van der Waals adhesion in gecko setae. *Proc. Natl Acad. Sci. USA* **99**, 12252–12256 (2002).
- Autumn, K. *et al.* Adhesive force of a single gecko foot-hair. *Nature* **405**, 681–685 (2000).
- Huber, G., Gorb, S. N., Spolenak, R. & Arzt, E. Resolving the nanoscale adhesion of individual gecko spatulae by atomic force microscopy. *Biol. Lett.* **1**, 2–4 (2005).
- Arzt, E., Gorb, S. & Spolenak, R. From micro to nano contacts in biological attachment devices. *Proc. Natl Acad. Sci. USA* **100**, 10603–10606 (2003).
- Arzt, E. Biological and artificial attachment devices: Lessons for materials scientists from flies and geckos. *Mater. Sci. Engin. C* **26**, 1245–1250 (2006).
- Spolenak, R., Gorb, S. & Arzt, E. Adhesion design maps for bio-inspired attachment systems. *Acta Biomater.* **1**, 5–13 (2005).
- Waite, J. H. Nature’s underwater adhesive specialist. *Chemtech* **17**, 692–697 (1987).
- Waite, J. H. Adhesion a la moule. *Integr. Comp. Biol.* **42**, 1172–1180 (2002).
- Waite, J. H. & Tanzer, M. L. Polyphenolic substance of *Mytilus edulis*: novel adhesive containing L-dopa and hydroxyproline. *Science* **212**, 1038–1040 (1981).
- Papov, V. V., Diamond, T. V., Biemann, K. & Waite, J. H. Hydroxyarginine-containing polyphenolic proteins in the adhesive plaques of the marine mussel *Mytilus edulis*. *J. Biol. Chem.* **270**, 20183–20192 (1995).
- Waite, J. H. & Qin, X. X. Polyphenolic phosphoprotein from the adhesive pads of the common mussel. *Biochemistry* **40**, 2887–2893 (2001).
- Yu, M. & Deming, T. J. Synthetic polypeptide mimics of marine adhesives. *Macromolecules* **31**, 4739–4745 (1998).
- Frank, B. P. & Belfort, G. Adhesion of *Mytilus edulis* foot protein 1 on silica: ionic effects on biofouling. *Biotechnol. Prog.* **18**, 580–586 (2002).
- Hwang, D. S., Yoo, H. J., Jun, J. H., Moon, W. K. & Cha, H. J. Expression of functional recombinant mussel adhesive protein Mgfp-5 in *Escherichia coli*. *Appl. Environ. Microbiol.* **70**, 3352–3359 (2004).
- Lee, B. *et al.* Rapid gel formation and adhesion in photocurable and biodegradable block copolymers with high DOPA content. *Macromolecules* **39**, 1740–1748 (2006).
- Lee, H., Scherer, N. F. & Messersmith, P. B. Single molecule mechanics of mussel adhesion. *Proc. Natl Acad. Sci. USA* **103**, 12999–13003 (2006).
- Whitesides, G. M. The origins and the future of microfluidics. *Nature* **442**, 368–373 (2006).
- Waite, J. H., Andersen, N. H., Jewhurst, S. & Sun, C. Mussel adhesion: finding the tricks worth mimicking. *J. Adhesion* **81**, 1–21 (2005).
- Dalsin, D. L., Hu, B.-H., Lee, B. P. & Messersmith, P. B. Mussel adhesive protein mimetic polymers for the preparation of nonfouling surfaces. *J. Am. Chem. Soc.* **125**, 4253–4258 (2003).

Supplementary Information is linked to the online version of the paper at www.nature.com/nature.

Acknowledgements We are grateful to the NIH and NASA for providing funding for this work. We thank J. Jureller and W. Russin for advice on optical imaging, B. Meyer for electron-beam lithography discussions, and V. Dravid and K. Shull for critical reading of the manuscript. Portions of this work used the NUANCE (EPIC, KECK-II and NIFTI) and biological imaging facilities at Northwestern University, the Nanobio facility at the University of Chicago, and the National Magnetic Resonance Facility at the University of Wisconsin-Madison.

Author Contributions P.B.M. planned the project, designed experiments, analysed data and wrote the manuscript. H.L. designed and performed experiments, analysed data and wrote the manuscript. B.P.L. designed and synthesized the polymer and wrote the manuscript.

Author Information Reprints and permissions information is available at www.nature.com/reprints. The authors declare competing financial interests: details accompany the full-text HTML version of the paper at www.nature.com/nature. Correspondence and requests for materials should be addressed to P.B.M. (philm@northwestern.edu).

METHODS

Synthesis of DMA. 20 g of sodium borate and 8 g of NaHCO₃ were dissolved in 200 ml of deionized water and bubbled with Ar for 20 min. 10 g of dopamine-HCl (52.8 mmol) was then added, followed by the dropwise addition of 9.4 ml of methacrylate anhydride (58.1 mmol) in 50 ml of THF, during which the pH of solution was kept above 8 with addition of 1 M NaOH as necessary. The reaction mixture was stirred overnight at room temperature with Ar bubbling. The aqueous mixture was washed twice with 100 ml of ethyl acetate and then the pH of the aqueous solution was reduced to less than 2 and extracted with 100 ml of ethyl acetate three times. The final three ethyl acetate layers were combined and dried over MgSO₄ to reduce the volume to around 50 ml. 450 ml of hexane was added with vigorous stirring and the suspension was held at 4 °C overnight. The product was recrystallized from hexane and dried to yield 9.1 g of grey solid. ¹H-nuclear magnetic resonance spectroscopy (400 MHz, DMSO-*d*/TMS): δ 6.64–6.57 (m, 2H, C₆H₂(OH)₂-), 6.42 (d, 1H, C₆H₂H(OH)₂-), 5.61 (s, 1H, -C(=O)-C(-CH₃)=CHH), 5.30 (s, 1H, -C(=O)-C(-CH₃)=CHH), 3.21 (m, 2H, C₆H₃(OH)₂-CH₂-CH₂(NH)-C(=O)-), 2.55 (t, 2H, C₆H₃(OH)₂-CH₂-CH₂(NH)-C(=O)-), 1.84 (s, 3H, -C(=O)-C(-CH₃)=CH₂). ¹³C-nuclear magnetic resonance spectroscopy (400 MHz, DMSO-*d*/TMS): δ 167.3 (s, 1C, -NH-C(=O)-C(CH₃)=CH₂), 145.0 (s, 1C, -NH-C(=O)-C(CH₃)=CH₂), 143.5–115.5 (6C, C₆H₃(O-C(=O)-CH₃)₂), 130.3 (s, 1C, -NH-C(=O)-C(CH₃)=CH₂), 41.0 (s, 1C, C₆H₃(OH)₂-CH₂-CH₂(NH)-C(=O)-), 34.6 (s, 1C, C₆H₃(OH)₂-CH₂-CH₂(NH)-C(=O)-), 18.7 (s, 1C, -C(=O)-C(-CH₃)=CH₂). Italics indicate the atom yielding the peak.

Synthesis of p(DMA-co-MEA). 12.5 ml of MEA was passed through a column packed with 30 g of Al₂O₃ to remove inhibitor. 7.5 g of purified MEA (57.9 mmol), 1.7 g of DMA (7.4 mmol), and 106 mg of azobisisobutyronitrile (0.64 mmol) were added to 20 ml of DMF in an airtight flask. The solution mixture was degassed through pump–freeze–thaw cycles three times. While sealed under vacuum, the solution was heated to 60 °C and stirred overnight. The reaction mixture was diluted with 50 ml of methanol and added to 400 ml of Et₂O to precipitate the polymer. After precipitating in DCM/Et₂O two more times and drying in the vacuum desiccator, 5.7 g of white, sticky solid was obtained. ¹H-nuclear magnetic resonance spectroscopy (400 MHz, CDCl₃/TMS): δ 6.81–6.70 (d, br, 2H, C₆H₂(OH)₂-), 6.58 (s, br, 1H, C₆H₂H(OH)₂-), 4.20 (s, br, 2H, CH₃-O-CH₂-CH₂-O-C(=O)-), 3.57 (s, br, 2H, CH₃-O-CH₂-CH₂-O-C(=O)-), 3.36 (s, br, 3H, CH₃-OCH₂-CH₂-O-C(=O)-), 2.69 (s, br, 2H, C₆H₃(OH)₂-CH₂-CH₂(NH)-C(=O)-), 2.39 (s, br, 1H, -O-C(=O)-CH(CH₂)-CH₂-), 2.14 (s, br, 2H, C₆H₃(OH)₂-CH₂-CH₂(NH)-C(=O)-), 1.93 (s, 3H, -NH-C(=O)-C(CH₃)(CH₂)-CH₂-), 1.68 (m, br, -O-C(=O)-CH(CH₂)-CH₂-), 0.98 (m, br, -NH-C(=O)-C(CH₃)(CH₂)-CH₂-). Analysis indicated a 1:6 molar ratio of DMA to MEA in the copolymer. Gel permeation chromatography in concert with multi-angle laser light scattering (Wyatt Technology), with mobile phase of 20 mM LiBr in DMF and Shodex-OH Pak columns: weight-average molecular mass = 252 kDa, polydispersity = 1.73. For control experiments, a catechol-free p(MEA) homopolymer (molecular mass (average) = 100 kDa, Scientific Polymer Products) was used.

Electron-beam lithography. Electron-beam resist (950 PMMA A3, MicroChem) was spin-coated (4,000 r.p.m., 40 s) on silicon wafer several times

until the resist thickness, as measured by ellipsometry (Woolam), reached 600–700 nm. The resist was patterned at 30 kV with an area dose of 650–800 μC cm⁻² using Quanta 600F (FEI). Resist development was performed for 1 min with a solution of methyl isobutyl ketone/isopropanol (1/3, v/v), followed by rinsing with water. The patterned substrates were treated with oxygen plasma (Harrick) for 30 s and repeated 2–3 times to remove residual resist completely from the exposed Si regions. The patterned substrates were then exposed to a triethoxyoctylsilane vapour for 30 min. PDMS was prepared as follows: 4 μl of Pt-catalyst (platinum-divinyl tetramethyl-disiloxane in xylene) and 4 μl of modulator (2,4,6,8-tetramethyl-2,4,6,8-tetravinylcyclotetrasiloxane) were added to a 7–8% vinylmethylsiloxane solution (3.5 g). The solution was subsequently mixed with a 25–30% methylhydrosiloxane (1 g) solution. Finally the solution was cured (80 °C) after spin-coating (1,000 r.p.m. for 1 min) onto the PMMA/Si master. The spin-coated substrate was covered either by thin cover glass for force measurements or sylgard-184 PDMS for other experiments such as optical imaging or x-ray photoelectron spectroscopy. Gecko adhesive was obtained by PDMS pattern lift-off and brief exposure to oxygen plasma (100 W, 30 s) and used within 2–3 h after plasma treatment. Geckel adhesive was prepared by dip-coating gecko adhesive in a 1 mg ml⁻¹ solution of p(DMA-co-MEA) in ethanol at 70 °C. Unstructured controls were fabricated in the same manner using flat PDMS, whereas structured controls were fabricated by dip-coating gecko adhesive in p(MEA) using the method described above.

X-ray photoelectron spectroscopy. The presence of p(DMA-co-MEA) and p(MEA) on PDMS surfaces was confirmed by X-ray photoelectron spectroscopy (Omicron) equipped with a monochromatic AlKα (1,486.8 eV) 300 W X-ray source and an electron gun to eliminate charge build-up.

Atomic force and optical microscopy. All force data were collected on an Asylum Mfp-1D AFM instrument (Asylum Research) installed on a Nikon TE2000 microscope. Spring constants of individual cantilevers (VeecoProbes, NP-20 tipless Si₃N₄ tips) were calibrated by applying the equipartition theorem to the thermal noise spectrum³⁰. Owing to the large forces exhibited by the adhesive, only tips exhibiting high spring constants (280–370 pN nm⁻¹) were used. Metal and metal-oxide-coated cantilevers were formed by sputter coating ~10 nm of Au or Ti (a native oxide formed at the Ti surface, TiO_x) using a Denton Vacuum Desk III. The surface composition of each cantilever was confirmed by time-of-flight secondary ion mass spectrometry, using a PHI-TRIFT III (Ga⁺, 15 keV, Physical Electronics). Cantilevers were treated by oxygen plasma (100 W, 150 mTorr) for 3 min before use. Force measurements were conducted either in millipore water or ambient (air) conditions at a cantilever pulling speed of 2 μm s⁻¹. In wet experiments, optical microscopic examination of the contact region indicated the absence of air bubbles trapped between nanopillars and on the nanopillar surface (not shown). Tapping-mode AFM images were obtained using a multimode Veeco Digital Instrument with a Si cantilever (resonance frequency of 230–280 kHz). Contact area was imaged by an inverted optical microscope using a 40× objective illuminated by a fibre-optic white light source perpendicular to the objective.

30. Hutter, J. L. & Bechhoefer, J. Calibration of atomic-force microscope tips. *Rev. Sci. Instrum.* **64**, 1868–1873 (1993).